Available online at www.sciencedirect.com
SCIENCE DIRECT
Journal of Sound and Vibration 294 (2006) 529–546
JOURNAL OF SOUND AND VIBRATION
www.elsevier.com/locate/jsvi

Torsional friction damper optimization

Shaochun Ye[a], Keith A. Williams[b,*]

[a]Department of Mechanical Engineering, The University of Alabama, 290 Hardaway Hall, Box 870276, Tuscaloosa, AL 35487-0276, USA
[b]Department of Mechanical Engineering, The University of Alabama, 164 Hardaway Hall, Box 870276, Tuscaloosa, AL 35487-0276, USA

Received 6 June 2005; received in revised form 7 November 2005; accepted 25 November 2005
Available online 13 February 2006

Abstract

A new approach for the analysis of friction dampers is presented in this work. The exact form of the steady-state solution for a friction damper implemented on a primary system is developed and numerical solutions are used to determine the optimum friction in a friction damper applied to a specific primary system. When compared to classical results presented by earlier authors, the new approach provides a more optimal solution. In addition, viscous damping in the primary system may be included with the new analysis approach. The ability to optimize a friction damper when viscous damping is included in the primary system is a significant improvement over earlier methods and shows potential for serving as a guide to realizing a more accurate estimate of the optimal damping for friction dampers.

1. Introduction

Control of torsional vibration is important to avoid failures in rotating shafts experiencing harmonic loads. Automotive engine crankshaft dampers and marine drive shafts are examples of applications that have benefited from research in the field of torsional vibration control. One well-known tool that is available for use in reducing torsional vibration is the dry friction damper, also known as a Lanchester damper. Design of Lanchester dampers was addressed in an early paper by Den Hartog and Ormondroyd [1]. These authors presented analytical and experimental work performed with the goal of determining the appropriate dry friction in a Lanchester damper to optimally damp the torsional vibration of a primary system. An important result of this work was an equation relating the optimal friction torque to the excitation torque acting on the primary system. In a more recent work, Ye and Williams [2,3] examined the use of a magneto-rheological (MR) fluid brake to control torsional vibrations. As shown by these authors, the MR fluid brake is essentially a variable-friction device, such that it should be readily applied to torsional vibration problems traditionally dealt with using a Lanchester damper. In the course of implementing the MR brake as a variable-friction Lanchester damper, it is important to understand some of the assumptions that went into the Den Hartog and Ormondroyd's [1] conclusions regarding the optimal friction in a Lanchester damper. The rest of this paper presents an analysis performed to determine the true optimal friction of a Lanchester damper. Modern computational tools allow for a new analysis that does not require the original assumptions used by Den

*Corresponding author. Tel.: +1 205 348 2605; fax: 1 205 348 6419.
E-mail address: kwilliams@coe.eng.ua.edu (K.A. Williams).

0022-460X/$ - see front matter © 2006 Elsevier Ltd. All rights reserved.
doi:10.1016/j.jsv.2005.11.025

Hartog and Ormondroyd [1]. In performing the analysis, the current authors were able to demonstrate that the result presented by Den Hartog and Ormondroyd [1] is not exact, but is sufficiently close to the exact solution such that the resulting primary system vibration reduction is quite close to that obtained with an optimally tuned Lanchester damper. The important result described in this work is thus the determination of the exact solution for the optimal friction torque in a Lanchester damper and, by extension, the validation of the assumptions of Den Hartog and Ormondroyd [1] in obtaining their estimate for that value.

In his text, Wilson [4] provides an excellent history of the topic of torsional vibration control. Apparently, torsional vibration became an issue when shaft failures became one of the limiting factors in the design of steam-powered marine vessels. According to Wilson, the problem became even more of an issue with the development of multi-cylinder internal combustion engines and the introduction of more complicated dynamics. The paper by Den Hartog and Ormondroyd [1] was another seminal work of the early 20th century. The Lanchester dampers studied by these authors work on the principle of an inertia coupled to a shaft-mounted hub through the use of spring-loaded friction plates. Varying the pre-load in the springs was used to modify the maximum friction force coupling the inertia to the hub. Based on certain assumptions regarding the nature of the solution, Den Hartog and Ormondroyd used energy methods to show that the optimum friction torque is directly proportional to the excitation torque acting on the main system. Eq. (13) of Den Hartog and Ormondroyd [1] describes the optimal friction torque, T, as

$$T = \sqrt{2}\frac{\pi}{4}M_0, \tag{1}$$

where M_0 is the excitation torque acting on the primary system. This result is also shown in other important works in the field, including Wilson [4], Tuplin [5], and the handbook compiled by Nestorides [6].

The MR fluid brake studied by Ye and Williams [2,3] works on a different principle than that of the classical dry friction damper. In an MR fluid, ferrous particles within the fluid align in long chains when subjected to a magnetic field, with a corresponding increase in the yield stress of the fluid, such that the fluid can be used in variable-friction applications. Numerous descriptions are available that describe the behavior of MR fluids, including the works by Jolly et al. [7] and Carlson et al. [8] and the text by Srinivasan and McFarland [9]. The MR fluid brake used by Ye an Williams [2,3] was commercially obtained. The actual internal construction of the device is proprietary, but the general design is thought to include a circular plate passing through an MR fluid-filled cavity between electromagnets. As current is passed through the electromagnets, the torque required to rotate the shaft of the MR brake relative to its housing is substantially increased. Srinivasan and McFarland [9] describe the behavior of an MR fluid device as being dominated by a variable dry friction, with some amount of viscous friction superimposed over the dry friction. To test the MR brake, Ye and Williams [3] mounted the brake to the end of a DC motor shaft as shown in Fig. 1. Fixed currents were applied to the MR brake coils and, for each fixed current, the motor voltage was ramped up and down a number of times. The MR brake housing was restrained from rotating by a load cell such that the MR brake torque was directly measured. The speed of the MR brake during the tests was determined using an encoder mounted inside the MR brake housing. The torque versus speed curves obtained for a number of different MR brake current levels are shown in Fig. 2. While there is a considerable amount of noise in the traces, the MR brake behavior is apparently dominated by dry friction and does not have a readily discernable viscous friction component in its response.

Based on the characterization of the MR brake as a dry friction device, Ye and Williams [3] implemented the brake on the simple torsional system shown in Fig. 3. The primary system was an 80 mm square plate with a thickness of approximately 30 mm. The plate was connected to a larger square plate by an 10.5 cm long 8 mm threaded shaft. The larger plate, in turn, had a 56 mm long arm mounted to a clevis bearing on the top of an electrodynamic shaker. Excitation of the shaker at constant linear acceleration thus resulted in base excitation of the primary system by a constant angular acceleration. This set-up was a slight variation from the one described by Den Hartog and Ormondroyd [1], where direct torque actuation was used. As such, some manipulation was required to apply Den Hartog and Ormondroyd's equation to determine the optimal friction. For the case of base excitation, if damping is neglected, the actual torque acting on the primary system, T_{exc}, is the product of the primary system shaft stiffness, K_{shaft}, and the base angular

Fig. 1. MR brake attached to DC motor for characterization tests.

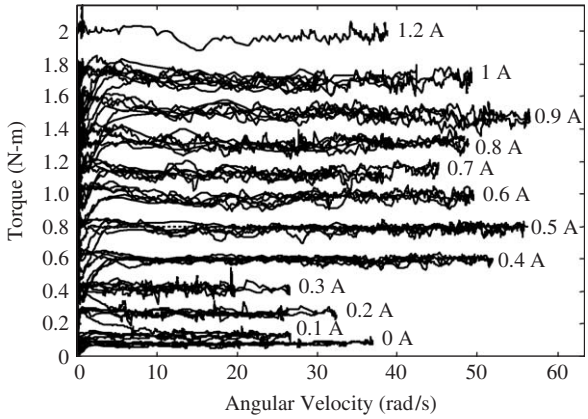

Fig. 2. Torque versus speed curves for the MR brake at different current levels.

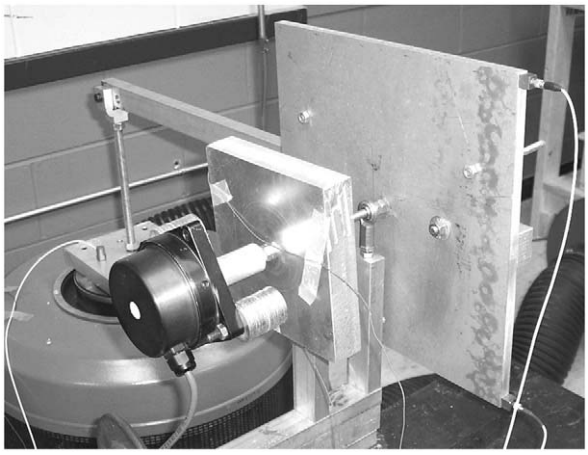

Fig. 3. MR brake applied to simple torsional system.

displacement, θ_{base}, according to

$$T_{exc} = K_{shaft}\theta_{base}. \tag{2}$$

If the system is harmonically excited with a fixed base angular acceleration, α_{base}, the amplitude of the base angular displacement is

$$|\theta_{base}| = \frac{|\alpha_{base}|}{\omega_{exc}^2}, \tag{3}$$

where ω_{exc} is the frequency of the base excitation. Den Hartog and Ormondroyd assumed that the maximum response of the primary system would occur at the natural frequency of the primary system. Therefore, combining Eqs. (1)–(3), the optimum friction torque for a harmonic base angular acceleration input is

$$T_{opt} = \sqrt{2}\frac{\pi}{4}K_{shaft}\frac{|\alpha_{base}|}{\omega_n^2}, \tag{4}$$

where ω_n is the natural frequency of the primary system. To test Eq. (4), Ye and Williams [3] controlled the shaker to produce constant acceleration frequency sweeps. The frequency response functions relating the resulting angular vibration amplitude of the primary system to the base acceleration excitation for different constant MR brake current levels are shown in Fig. 4 for shaker acceleration sweeps at 5 g. The 5 g shaker acceleration amplitude corresponds to a base peak angular acceleration of 87 rad/s^2.

In Fig. 4, the frequency response with the minimum peak amplitude occurs with an MR brake current of 0.75 A. Using Fig. 2, the current level corresponds to an MR brake torque of approximately 1.25 N m. It is important to note that the maximum response occurs at a frequency of 19 Hz, which is lower than the unloaded primary system's natural frequency of 21.5 Hz.

To compare the experimental optimal brake torque to the torque predicted by Eq. (4), the excitation frequency and shaft stiffness are necessary. The frequency of the peak response is readily obtained by examining the figure and is approximately 19 Hz, or $\omega_{exc} = 119.4$ rad/s. The shaft stiffness was determined using the frequency response of the primary system with no MR brake attached. The resulting resonant frequency of 21.5 Hz and the approximate inertia of the primary system ($J_p = 0.0088$ kg m^2) resulted in an approximate shaft stiffness of $K_{shaft} = 160.6$ N m/rad. The shaft stiffness and base angular acceleration, together with frequency of the peak response, resulted in a predicted optimal friction torque of approximately 0.9 N m. The predicted optimum friction torque is thus noticeably less than the optimum experimental friction torque, which was approximately 1.25 N m, as noted above.

As a first attempt at implementing a novel torsional vibration control device, the error between the predicted and experimental optimal torques was judged to be satisfactory, particularly given the implementation of a nonlinear system such as the MR brake. However, the error was significant enough to

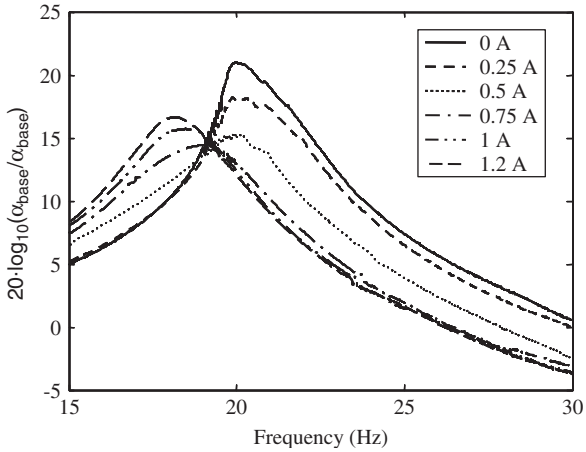

Fig. 4. Primary system frequency responses for $|\alpha_{base}| = 87$ rad/s^2: —, 0 A; - - -, 0.25 A; · · · ·, 0.5 A; – · –, 0.75 A; – · · –, 1.0 A; – – –, 1.2 A.

warrant further investigation into the assumptions that went into the development of Eq. (4). In particular, Den Hartog and Ormondroyd [1] made the assumption that the hub of the Lanchester damper undergoes purely sinusoidal motion. In addition, these authors assumed that the maximum response amplitude will occur at the natural frequency of the primary system. These assumptions were supported by experimental evidence and, as it turns out, are quite acceptable. However, in using these assumptions, Den Hartog and Ormondroyd did not consider the effect that implementation of the damper would have on the dynamics of the primary system. In seeking to understand one possible reason for the difference between the predicted and experimental results demonstrated by Ye and Williams [3], the current authors decided to examine an alternate approach to the determination of the optimal torque in a dry friction damper. Specifically, the authors chose to search for an exact solution for the optimal torque in a dry friction damper applied to a primary system of finite inertia and finite shaft stiffness. The rest of this paper describes the results of that investigation. The next section of this paper provides a brief description of the analysis provided by Den Hartog and Ormondroyd [1]. That is followed by an alternate approach to describing the motion of the complete system, including the inertia and shaft stiffness for the primary system. The use of optimization approaches to determine the exact solution is then described and results for the optimum friction torque for a particular primary system are presented.

2. Optimal solution of Den Hartog and Ormondroyd [1]

As discussed previously, Den Hartog and Ormondroyd [1] presented an energy analysis approach to the determination of the optimum friction torque in a Lanchester damper. These authors considered a torsional system represented by two inertias mounted on a common shaft. At one end, there is a large flywheel. At the other end is an inertia that represents the combined inertia of "rotating and reciprocating parts of the gas or Diesel engine [1]." A dry friction damper is connected to the outside of the lumped engine inertia. The damper consists of an inertial ring connected to a hub by dry friction elements. The objective of Den Hartog and Ormondroyd [1] was to determine the appropriate frictional torque in the damper to dissipate the maximum amount of energy per cycle from the system. Certain assumptions were made in order to perform the analysis. The assumptions were: (1) the primary inertia is acted on by a sinusoidal force; (2) the resultant motion of the primary inertia is a pure sinusoid; (3) there is a 90° phase shift between the torque excitation and the resultant motion of the primary inertia at resonance, a condition achieved with negligible damping in the primary system.

In addition, Den Hartog and Ormondroyd assumed that the maximum energy dissipation would occur at the natural frequency of the primary system. Implicit in this assumption is the further assumption that implementation of the friction damper does not significantly affect the natural frequency of the primary system. Therefore, the ratio of the damper inertia to the primary system inertia is implicitly assumed to be very small. The largest amplitude of the primary inertia will thus occur at the natural frequency of the primary system. The torque excitation acting on the primary system is

$$T_{\text{exc}}(t) = T_0 \sin(\omega t),$$

where ω is the natural frequency of the primary system. The resulting angular displacement of the primary inertia, θ_p, is thus

$$\theta_p(t) = \theta_{p_0} \sin(\omega t - 90^o) = -\theta_{p_0} \cos(\omega t). \tag{5}$$

The work per cycle, W_{add}, done on the primary system by the torque T_{exc}, is

$$W_{\text{add}} = \int_0^{2\pi/\omega} T_{\text{exc}}(t)\dot{\theta}_p(t)\,\mathrm{d}t = \pi T_0 \theta_{p_0}. \tag{6}$$

Depending on the magnitude of the maximum friction torque in the damper, $T_{f,\max}$, three types of motion are possible:

1. *Complete stick*: if the acceleration of the primary inertia, I_p, is always less than $T_{f,\max}/I_d$, then the friction damper inertia, I_d, never slips but instead tracks the motion of I_p.

2. *Complete slip*: the friction damper slips continuously.
3. *Stick-slip*: I_d tracks the motion of I_p during part of the cycle and slips during the rest of the cycle.

Example motions for Case 2 and Case 3 are shown in Figs. 5 and 6. Note that Figs. 5 and 6 are actually more exact solutions than those assumed by Den Hartog and Ormondroyd [1]. For example, in Fig. 5, while the solutions appear to be a pure sinusoid and a set of straight lines, the actual solutions are slightly different, as will be explained in the following section of this work.

For the first case, the energy dissipated by the friction damper is zero. For the second case, complete slip, Den Hartog and Ormondroyd [1] showed that the energy dissipated per cycle by the friction damper, W_{diss}, is

$$W_{\text{diss}} = 4T_{f,\max}\theta_{p_0}\sqrt{1-\left(\frac{\pi}{2}\frac{T_{f,\max}}{I_p\omega^2\theta_{p_0}}\right)^2}. \tag{7}$$

For a stable system at steady state, the added energy, W_{add}, and W_{diss} are equal. Therefore, by equating Eqs. (6) and (7), Den Hartog and Ormondroyd [1] described W_{diss} as an explicit function of $T_{f,\max}$, up to the point where stick-slip begins to occur. At some point prior to the onset of stick-slip, the slope of the function $W_{\text{diss}}(T_{f,\max})$ goes to zero. This point is considered as the point where the friction torque provides the maximum amount of energy dissipation per cycle and is thus the point of optimum friction in the damper. $W_{\text{diss}}(T_{f,\max})$ is plotted with a solid line in Fig. 7. The energy dissipated per cycle with complete stick is zero, as noted previously, and is plotted as the solid line through the circles in Fig. 7. The start of this line is at the

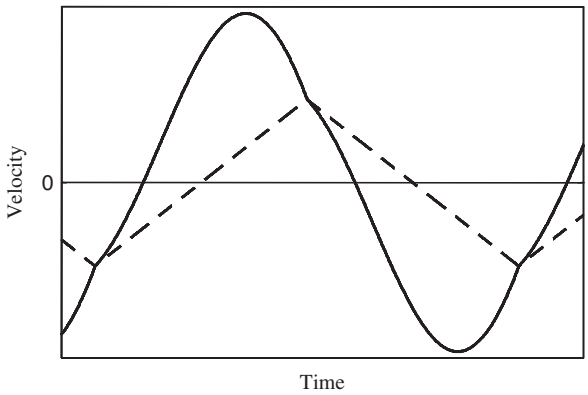

Fig. 5. Continuous slipping of the friction damper during a cycle.

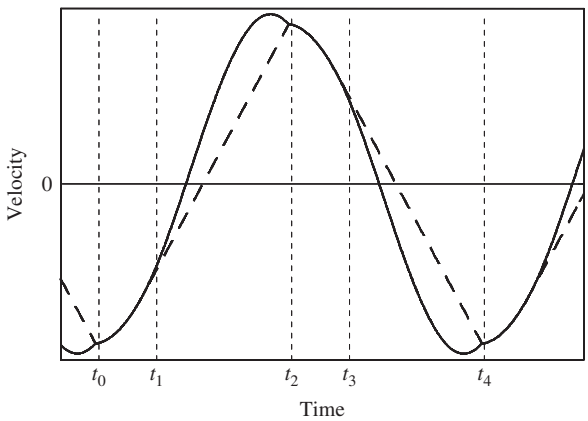

Fig. 6. Stick-slip motion of the friction damper during a cycle: —, primary system velocity; ----, damper velocity.

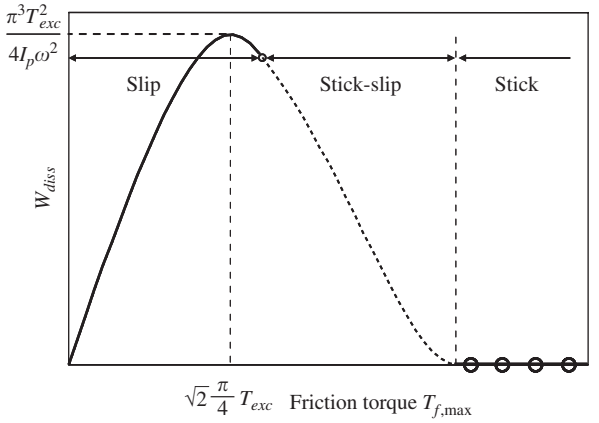

Fig. 7. Work dissipated by friction damper as a function of friction torque: —, W_{diss} during slip; …, W_{diss} during stick-slip; ⊖, W_{diss} during stick.

friction torque required to create the locked condition and extends continuously to higher friction levels along the horizontal axis. Between these two plots, there is a dashed trace. That trace represents $W_{\text{diss}}(T_{f,\max})$ for the case of friction levels sufficient to produce the stick-slip motion, but insufficient to produce a complete lock over the entire cycle. The stick-slip trace shown in Fig. 7 is the result of an analytical effort that will be described later in this work. The important issue to note is that the approach taken by Den Hartog and Ormondroyd [1], in describing $W_{\text{diss}}(T_{f,\max})$ as an explicit function during the slip phase of the plot, does have an actual maximum point, which is obtained at a friction level of

$$T_{f,\text{opt}} = \sqrt{2}\frac{\pi}{4} T_{\text{exc}}, \tag{8}$$

where T_{exc} is the amplitude of the excitation torque acting on the primary system. As such, the result obtained by Den Hartog and Ormondroyd [1] indicates that the optimum friction torque in a Lanchester damper is related only to the amplitude of the sinusoidal torque acting on the primary system. The issue becomes one of whether or not the expression given in Eq. (8) is valid when the assumptions are relaxed. This is examined in a new approach to the analysis of a friction damper applied to a primary system as presented in the next section of this work.

3. Analysis with relaxed assumptions

The alternate approach to the determination of the optimal friction torque in a friction damper considers a system consisting of finite damper and primary system inertias with a base angular displacement applied to the primary system through the primary system's stiffness. In addition, a provision for including damping in the primary system is included. A schematic of the system is shown in Fig. 8. In this figure, for the sake of simplicity, the system is represented as a linear system, rather than a torsional system. The expression for the base angular displacement is

$$\theta_b(t) = \theta_{b_0} \sin(\omega t + \phi), \tag{9}$$

where the phase angle ϕ is included only to ensure a completely general solution. For the system shown in Fig. 8, with the displacement excitation amplitude θ_{b_0}, Eqs. (1) and (2) can be combined to yield the optimum friction torque according to Den Hartog and Ormondroyd

$$T_{f,\text{opt}} = \sqrt{2}\frac{\pi}{4} K_P \theta_{b_0}. \tag{10}$$

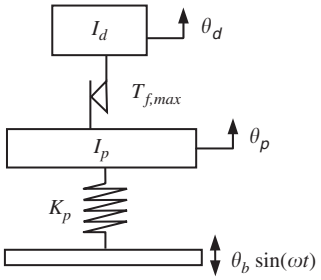

Fig. 8. Base excited system with friction damper applied.

Further, according to the analysis of Den Hartog and Ormondroyd [1], the expressions for the work dissipated per cycle and the maximum amplitude of the primary system's displacement are

$$W_{\text{diss}} = \frac{\pi^3 K_p^2 \theta_{b_0}^2}{4 I_p \omega^2} \quad \text{and} \quad |\theta_p| = \left(\frac{\pi}{2}\right)^2 \frac{K_p \theta_{b_0}}{I_p \omega^2}. \tag{11,12}$$

It should be noted that Den Hartog and Ormondroyd [1] assumed that the maximum response of the primary system would occur at the primary system's natural frequency. As such, for determination of W_{diss} and $|\theta_p|$ using Eqs. (11) and (12), ω is assumed to be the primary system's natural frequency, $\sqrt{K_p/I_p}$.

3.1. Solution for locked inertias

In the new approach, for any given combination of $\{\theta_{b_0}, T_{f,\max}, \omega\}$, the equations of motion for both the damper and the primary system are obtained and then solved. Because of the discontinuity introduced by the friction element in the system, piecewise solutions are necessary. As described previously, three distinct solution domains must be considered, complete stick/lock, complete slip, and stick-slip. The complete stick/lock and complete slip cases will also be referred to as the "stick-only" and "slip-only" cases, respectively. For the case of complete stick, the equations of motion are

$$\ddot{\theta}_p(t) = \frac{K_p[\theta_b(t) - \theta_p(t)] + C_p[\dot{\theta}_b(t) - \dot{\theta}_p(t)]}{I_p + I_d}, \tag{13}$$

$$\ddot{\theta}_d(t) = \ddot{\theta}_p(t), \tag{14}$$

where C_p is the damping of the primary system and θ_b is the instantaneous value of the angular displacement input. Eqs. (13) and (14) hold only if the damper remains locked to the primary system for the complete cycle. The condition required for this to occur is that the friction torque be greater than the product of the damper inertia and the maximum acceleration given by Eq. (13). That is,

$$T_{f,\max} > I_d \ddot{\theta}_p\Big|_{\max}. \tag{15}$$

In Eq. (15), $T_{f,\max}$ refers to the maximum friction torque that can be developed in the friction damper. If Eq. (15) holds, the primary system and damper combination is a simple second-order system and the steady-state solution for the primary system displacement is

$$\theta_p(t) = \theta_{b_0} A_{\text{stick}} \sin(\omega t + \phi + \phi_{\text{stick}}), \tag{16}$$

where

$$A_{\text{stick}} = \sqrt{\frac{K_p^2 + C_p^2 \omega^2}{(K_p - (I_p + I_d)\omega^2)^2 + C_p^2 \omega^2}}, \tag{17}$$

$$\phi_{\text{stick}} = \tan^{-1}\left(\frac{C_p\omega}{K_p}\right) - \tan^{-1}\left(\frac{C_p\omega}{K_p - (I_p + I_d)\omega^2}\right). \tag{18}$$

The solution for $\theta_d(t)$ follows from Eq. (16), with the minor modification that an offset angle may exist between $\theta_p(t)$ and $\theta_d(t)$, depending on the initial positions of the two inertias. Note that the transient component of the complete solution is neglected in Eq. (16), as the main interest is in the steady-state solution at this point. In order for the solution given by Eq. (16) to hold,

$$T_{f,\max} > \omega^2\theta_{b_0}A_{\text{stick}}(I_p + I_d) \tag{19}$$

must be satisfied. Eq. (19) is a modification of Eq. (15) using the knowledge that, at steady state, the amplitude of the acceleration will be $\omega^2\theta_{b_0}A_{\text{stick}}$. In this case, the determination of the steady-state amplitude would be trivial, as the system would be linear. An interesting situation occurs if the primary system is undamped. In this case, Eq. (17) would imply an unstable solution if the system were excited at the natural frequency $\sqrt{K_p/(I_p + I_d)}$. In this case, however, the amplitude of vibration would rise up to a point where the condition given by Eq. (19) would be violated. This indicates that the complete stick state will never occur for an undamped primary system when the excitation frequency is $\sqrt{K_p/(I_p + I_d)}$, regardless of the magnitude of $T_{f,\max}$. As such, in the theoretical case of an undamped primary system, there will exist some frequency below the natural frequency of the combined system where the onset of slip will occur. At immediately higher frequencies, stick-slip behavior will occur and may progress to slip-only behavior. For the sake of simplicity, before considering the stick-slip case, the slip-only case will be examined.

3.2. Solution for complete slip

For a given combination of $\{\theta_{b_0}, T_{f,\max}, \omega\}$, if Eq. (19) is not satisfied, the system steady state will be either complete slip or stick-slip. In considering the case of complete slip, a more complex solution approach is required. In this case, the equations of motion for the primary system and damper inertia are

$$\ddot{\theta}_p = \frac{K_p}{I_p}(\theta_b - \theta_p) + \frac{C_p}{I_p}(\dot{\theta}_b - \dot{\theta}_p) - T_f, \quad \ddot{\theta}_d = \frac{T_f}{I_d}, \tag{20,21}$$

where

$$T_f = \begin{cases} T_{f,\max}, & (\dot{\theta}_p - \dot{\theta}_d) > 0, \\ -T_{f,\max}, & (\dot{\theta}_p - \dot{\theta}_d) < 0. \end{cases} \tag{22}$$

For these equations, a steady-state solution will exist that will be periodic and will be mirrored about the horizontal axis. However, the steady-state solution will actually be composed of a sum of solutions which actually are a series of repeated transient solutions. That is to say, the solutions for $\theta_p(t)$ and $\theta_d(t)$ are not simple harmonic functions with fixed amplitudes. A solution to $\theta_p(t)$ can be determined for the part of the cycle when $(\dot{\theta}_p - \dot{\theta}_d) > 0$, such that $T_f = T_{f,\max}$. In Fig. 5, this is the part of the cycle when the nearly sinusoidal response of the primary system is above the apparently linear response of the damper. During this part of the cycle, the solutions are

$$\theta_p(t) = \theta_b A_{\text{slip}} \sin(\omega t + \phi + \phi_{\text{slip}}) - \frac{T_{f,\max}}{K_p} + e^{-\zeta\omega_n t}[B_1 \sin(\omega_d t) + B_2 \cos(\omega_d t)] \tag{23}$$

and

$$\theta_d(t) = \frac{T_{f,\max}}{2I_d}t^2 + C_1 t + C_2, \tag{24}$$

where

$$\omega_n = \sqrt{\frac{K_p}{I_p}}, \quad \zeta = \frac{C_p}{2\sqrt{K_p I_p}}, \quad \omega_d = \omega_n\sqrt{1-\zeta^2}, \quad A_{\text{slip}} = \sqrt{\frac{K_p^2 + C_p^2\omega^2}{(K_p - I_p\omega^2)^2 + C_p^2\omega^2}},$$

$$\phi_{\text{slip}} = \tan^{-1}\left(\frac{C_p\omega}{K_p}\right) - \tan^{-1}\left(\frac{C_p\omega}{K_p - I_p\omega^2}\right).$$

The coefficients B_1, B_2, C_1, and C_2 are determined by the initial conditions of the primary system and damper displacement and velocity. In this case, the initial conditions must be determined every half-cycle. That is, the initial conditions for the above solution are given by the position and velocity at time t_0 in Fig. 5. The two solutions just described above are then valid until the time t_1, at which point a new pair of solutions is required. These new solutions are

$$\theta_p(t) = \theta_b A_{\text{slip}}\ \sin(\omega t + \phi + \phi_{\text{slip}}) + \frac{T_{f,\max}}{K_p} + \mathrm{e}^{-\zeta\omega_n t}[B_1\ \sin(\omega_d t) + B_2\ \cos(\omega_d t)], \tag{25}$$

$$\theta_d(t) = \frac{-T_{f,\max}}{2I_d}t^2 + C_1 t + C_2, \tag{26}$$

where the coefficients B_1, B_2, C_1, and C_2 are now determined using Eqs. (25) and (26) and the primary system and damper displacement and velocity at time t_1, as provided by the solution to Eqs. (23) and (24) during the prior half-cycle. This process is repeated for every half-cycle of the solution.

At this point, if an appropriate set of initial conditions is picked for time $t = 0$, then the above solutions can be applied in a piecewise fashion. The particular choice of a solution pair, Eqs. (23) and (24) or Eqs. (25) and (26), depends on the chosen initial relative velocities. The solution then continues according to either Eqs. (23) and (24) or Eqs. (25) and (26) until such a point where the velocities of the two inertias are equal, for example, at time t_0 or t_1 in Fig. 5. At this instant, the solution form would switch and the instantaneous positions and velocities would be used as the initial conditions for the next solution step; if Eqs. (23) and (24) were originally used, the solution would switch to Eqs. (25) and (26), and vice versa. One important point about this solution approach is that an appropriate set of initial conditions is required, due to the assumption of the slip condition. For example, if an initial condition is chosen where the two inertias are matched in velocity and the initial torque acting on the primary system is sufficiently small, the friction torque will be sufficient to cause stick and the solutions given by Eqs. (23) and (24) and Eqs. (25) and (26) will be invalid. In order to realize a truly general solution approach, a stick-slip form of solution is required. To this end, a solution for the system under stick-slip behavior is considered next.

3.3. Stick-slip solution

For the case of stick-slip, as shown in Fig. 6, during part of the cycle, the two inertias are locked with matched velocities. For the other part of the cycle, the two inertias slip. During the slipping part of the cycle, the damper is subject to simple constant force excitation. As with the slip solutions detailed above, the stick-slip solutions must be performed in a piecewise manner. In this case, however, four solutions are required per half-cycle: a solution for the motion of each inertia during the locked portion of the cycle, and a solution for the motion of each inertia during the slip portion of the cycle. For example, in Fig. 6, the two inertias become locked at time t_0. If the velocities and positions of the two inertias are known at this instant, then the solution for the resulting motion will be given by the equations

$$\theta_p(t) = \theta_b A_{ss}\ \sin(\omega t + \phi + \phi_{ss}) + \mathrm{e}^{-\zeta_{ss}\omega_{n,ss}t}[B_1\ sin(\omega_{d,ss}t) + B_2\ \cos(\omega_{d,ss}t)] \tag{27}$$

and

$$\theta_d(t) = \theta_d(t_0) + \theta_p(t), \tag{28}$$

where

$$\omega_{n,ss} = \sqrt{K_p/I_p + I_d}, \quad \zeta_{ss} = C_p/\sqrt{K_p(I_p + I_d)} \quad \text{and} \quad \omega_{d,ss} = \omega_{n,ss}\sqrt{1-\zeta_{ss}^2}.$$

A_{ss} and ϕ_{ss} are identical to A_{stick} and ϕ_{stick} in Eqs. (17) and (18), respectively, and B_1 and B_2 are determined using the initial position and velocity of the primary system. The start of lock occurs when the two angular velocities are matched and the acceleration of the locked inertias is insufficient to break the friction in the damper. With a sufficiently large torque acting on the primary system, at some time t_1 the acceleration of the two will demand more friction torque than is available and sliding will start. The solution for the two inertias' motions will then be identical to the solutions given in Eqs. (23) and (24) above. The positions and velocities of the two inertias at time t_1 are necessary to solve for the new coefficients, B_1, B_2, C_1, and C_2. The two solutions will continue to be valid until time t_2, at which point the velocities of the two inertias will match and the acceleration of the primary system will be sufficiently small as to allow for lock to occur. This point will represent a half-cycle of the solution. To continue the solution and complete the cycle, the locked condition solution, as given in Eqs. (27) and (28) is used again, but the coefficients B_1 and B_2 are determined by the position and velocity of the primary inertia at time t_2. The magnitude of the acceleration of the primary inertia will again grow and slip will occur at some time t_3. The positions and velocities of the two inertias at this instant can then be used to determine the motion during the rest of the cycle, according to Eqs. (25) and (26). The cycle will end when lock again occurs at some time t_4. The use of Eqs. (23) through (28) to determine the trajectory of the two inertias is possible for any set of arbitrary initial conditions. In addition, the solution is exact and does not require numerical integration or approximations.

Certain characteristics of the solutions can be noted. First, if the resonant frequency is defined as the point of maximum response of the primary system, then the resonant frequency will vary with the friction in the damper. This is intuitive, in that a locked damper will drop the natural frequency of the combined system and at the other extreme, with zero friction between the damper and the primary system, the primary system's natural frequency would not be modified at all. The actual resonant frequency thus varies between these two extremes, starting at the primary system's unmodified natural frequency and reducing in frequency with increasing friction, until the locked natural frequency is obtained. This behavior is seen in the experimental results of Fig. 4. The definition of the optimum friction is now a more complicated issue. For the purposes of this work, the optimum friction is taken to be the friction that minimizes the maximum displacement of the primary system across all frequencies. In this sense, the definition of the optimum friction is similar to the definition of the infinity-norm used in H_∞ control theory.

In examining the question of the optimum friction in a Lanchester damper, the chief consideration is the steady-state response. Given the intricacies of the solution as pointed out in the previous paragraph, one way to determine the optimum friction is to grid a reasonable space in terms of friction and frequency. For each $\{T_{f,\max}, \omega_{\text{exc}}\}$ pair, a reasonable approximation to the steady-state response is to solve the above equations for a sufficient number of cycles. Automation can be achieved by placing the solution inside of the "while" loop and continuing the solution until the variation in the peak values across any given integer number of periods is below some predefined maximum. This process could be performed for a fixed primary system (inertia, stiffness, and damping) and a fixed damper inertia. The $\{T_{f,\max}, \omega_{\text{exc}}\}$ space could be reduced to frequencies between the extreme "stick" and "slip" natural frequencies of the primary system as defined above. However, to a certain degree, the use of the time-domain simulation approach effectively adds a third dimension to the gridded space, in that the time at which a reasonable approximation to steady state occurs is unknown. Some alternate approach that provides the steady-state solution without the requirement for extensive simulation is desirable.

3.4. Direct determination of steady-state solution

To work directly with the steady-state solution, another approach was developed that takes advantage of two characteristics of the steady-state solution: first, the steady-state solution is periodic with period $2\pi/\omega$. This is a result of the primary system being excited at the frequency ω. In addition, at steady state, every half-period of the response is a mirror image of the prior half-cycle. That is, any half-period of motion may be

"cut" out of the solution, inverted, and translated back in time by one half-period. The cut, inverted, and translated signal will then match identically the signal for that prior half-period of time. At steady state, therefore, from one period to the next, the responses differ only in sign. Because of this characteristic, only a half-period of the solution must be considered. For example, it is sufficient to consider the solution during the half-period from the time t_0 to time t_2 in Fig. 6.

In considering this half-period of signal, another characteristic is apparent: $\dot{\theta}_p(t_0) = -1\dot{\theta}_d(t_2)$. Also, as θ_d does not enter into the equations of motion, $\theta_d(t_0)$ can be arbitrarily selected such that $\theta_d(t_0) = \theta_p(t_0)$. If this is done, the collection of equations describing the motion through the half-period are as follows:

For $t_0 \leqslant t \leqslant t_1$,

$$\theta_p(t) = \theta_{b_0} A_{ss} \sin(\omega t + \phi + \phi_{ss}) + e^{-\zeta_{ss}\omega_{n,ss}t}[B_1 \sin(\omega_{d,ss}t) + B_2 \cos(\omega_{d,ss}t)], \tag{29}$$

$$\theta_d(t) = \theta_p(t), \tag{30}$$

where B_1 and B_2 are determined using $\theta_p(t_0)$ and $\dot{\theta}_p(t_0)$.

For $t_1 \leqslant t \leqslant t_2$,

$$\theta_p(t) = \theta_{b_0} A_{\text{slip}} \sin(\omega t + \phi + \phi_{\text{slip}}) - \frac{T_{f,\max}}{K_p} + e^{-\zeta\omega_n t}[D_1 \sin(\omega_d t) + D_2 \cos(\omega_d t)], \tag{31}$$

$$\theta_d(t) = \frac{T_{f,\max}}{2I_d} t^2 + C_1 t + C_2, \tag{32}$$

where C_1, C_2, D_1, and D_2 are determined based on $\theta_p(t_1)$ and $\dot{\theta}_p(t_1)$. $\theta_d(t_1)$ and $\dot{\theta}_d(t_1)$ are identical to $\theta_p(t_1)$ and $\dot{\theta}_p(t_1)$ at this point and are thus unnecessary.

After a good deal of algebraic manipulation, it is possible to express the coefficients B_1, B_2, C_1, C_2, D_1, and D_2 in terms of the appropriate functions for $\theta_p(t)$, $\dot{\theta}_p(t)$, $\theta_d(t)$, and $\dot{\theta}_d(t)$. In addition, the phase angles ϕ_{stick} and ϕ_{ss} and the magnitude ratios A_{ss} and A_{slip} can be expressed in terms of the fundamental parameters of the system, I_p, I_d, K_p, and C_p. As such, given the initial conditions $\{\theta_p(t_0), \dot{\theta}_p(t_0)\}$ and the phase angle of the base excitation, ϕ, it is possible to determine the solutions for $\theta_p(t)$ and $\theta_d(t)$ over the subsequent half-cycle.

As noted previously, for a given excitation amplitude θ_{b_0}, the frequency at which stick-slip behavior will start, $\omega_{\text{onset},ss}$, can be determined using the inequality expressed in Eq. (19). For frequencies above $\omega_{\text{onset},ss}$, stick-slip behavior will occur until a frequency $\omega_{\text{onset,slip}}$, at which frequency the response will become slip-only. $\omega_{\text{onset,slip}}$ is not easily determined and is found only by considering the stick-slip solutions and finding the frequency at which these solutions are no longer valid. For the moment, the assumption is made that an appropriate combination of $\{\theta_{b_0}, T_{f,\max}, \omega\}$ has been chosen such that stick-slip behavior will occur. In this case, the steady-state solution is achieved by an appropriate choice of the unknowns $\dot{\theta}_p(t_0)$, $\theta_p(t_0)$, and ϕ. If these values can be chosen such that the solutions to Eqs. (29)–(32) satisfy the constraints

$$t_2 = \frac{\pi}{\omega_{\text{exc}}}, \quad \dot{\theta}_p(t_2) = -1\dot{\theta}_p(t_0), \quad \dot{\theta}_d(t_2) = -1\dot{\theta}_d(t_0) \tag{33,34,35}$$

and

$$I_d\ddot{\theta}_p(t_1) = T_{f,\max}, \tag{36}$$

then the steady-state solution will have been found. For example, suppose some $\{\theta_{b_0}, T_{f,\max}, \omega\}$ where ω is just above $\omega_{\text{onset},ss}$, such that stick-slip behavior is anticipated. The time t_0 is arbitrarily chosen as $t_0 = 0$. A set of initial conditions $\{\theta_p(0), \dot{\theta}_p(0)\}$ and the phase ϕ are then chosen. If the damper and primary system inertias are assumed to be initially at a matched speed and velocity, then the second derivative of Eq. (29) is solved to determine the time t_1 such that Eq. (36) is satisfied. Eqs. (31) and (32) will be then solved until the velocities again match. If the time at which the velocities match is equal to t_2, as given by Eq. (33) and if, at this time, the velocities satisfy the constraints given by Eqs. (34) and (35), then the steady-state solution will have been realized.

A general approach is thus to pick a set of initial conditions, solve for t_1 using the second derivative of Eq. (29), switch the solution to Eqs. (31) and (32) until time $t_2 = \pi/\omega_{\text{exc}}$, and then examine to see if the constraints given by Eqs. (34) and (35) are met (with the implicit constraint $\{\dot{\theta}_d(t_2), \dot{\theta}_p(t_2)\}$, as the two inertias

start with matched velocities). To determine t_1 using the second derivative of Eq. (29), a nonlinear equation solver must be used. The trick then is to determine an appropriate set of initial conditions $\{\theta_p(0), \dot{\theta}_p(0)\}$ and the excitation phase angle ϕ. These values can be iterated on using a nonlinear equation solver operating on the set of variables $\{\theta_p(0), \dot{\theta}_p(0), \phi\}$. The general approach is thus to arrange the nonlinear equations such that the results will be algebraic in $\{\theta_p(0), \dot{\theta}_p(0), \phi\}$. Given a starting guess for $\{\theta_p(0), \dot{\theta}_p(0), \phi\}$, the time t_1 is first solved for. The values $\{\theta(t_2), \theta_d(t_2), \theta_p(t_2), \dot{\theta}_p(t_2)\}$ are then determined and examined to see if the constraints are satisfied. If not, then the equation solver perturbs the "guess" and repeats the process iteratively until the constraints are satisfied to within some maximum error.

Before continuing on with a discussion of the results of an analysis using the above approach, it is appropriate to review the goal of the work. The ultimate goal is the determination of the optimum friction in the damper such that the maximum steady-state response of the primary system is minimized. The question to be answered, then, is:

> Given some primary system composed of an inertia I_p and stiffness K_p, and mounted with a friction damper of inertia I_d, what is the friction in the damper, $T_{f,\max}$, that will minimize the maximum response of I_p when subjected to a harmonic base excitation with amplitude θ_{b_0}?

The determination of the optimum friction thus requires the solution of the steady state $\theta_p(t)$ for each of a collection of frequencies and friction levels. As described previously, if complete stick occurs for the steady-state response, determination of the steady-state amplitude is trivial, as the system is linear. However, at each $\{T_{f,\max}, \omega\}$ point in the space where the stick-slip or complete slip behavior occurs, an appropriate $\{\theta_p(0), \dot{\theta}_p(0)\}$ and ϕ must be determined to provide the steady-state response. By determining the explicit solution for $\theta_p(t)$ and $\theta_d(t)$ over the different intervals $0 \leqslant t < t_1$ and $t_1 \leqslant t < t_2$, the appropriate $\{\theta_p(0), \dot{\theta}_p(0)\}$ and ϕ to realize a steady-state response for a given $\{\theta_{b_0}, T_{f,\max}, \omega\}$ can be obtained. The maximum steady-state value of $\theta_p(t)$ is then readily obtained for this $\{\theta_{b_0}, T_{f,\max}, \omega\}$ combination. The nonlinear equation solver routine *fsolve* in the *Optimization Toolbox* of the Mathworks product *Matlab*® was used to realize the steady-state solutions according to this approach. The results of such an analysis are presented in the following section.

4. Results

To determine the optimum damper friction for a specific system, a two-dimensional space of frequency and friction is proposed. The maximum steady-state displacement $\theta_p(t)$ is then determined for a fine grid in this space. The maximum responses for each increment of friction are collected and examined. The friction level that results in the minimum value of this set of maximum responses is then taken as indicating the optimum amount of friction in the friction damper.

In order to compare the optimum response according to this new approach to the response specified by Den Hartog and Ormondroyd [1], an undamped primary system was chosen, with an inertia $I_p = 1\,\mathrm{kg\,m^2}$ and a stiffness $K_p = 25\,\mathrm{N\,m/rad}$. The optimum friction for each of three different friction damper inertias was then determined. The different friction damper inertias were $I_d = 0.1$, 0.2, and $0.5\,\mathrm{kg\,m^2}$, with corresponding mass ratios of $\mu = 0.1$, 0.2, and 0.5, respectively. The use of a mass ratio $\mu = 0.5$ may not be practical, but it was chosen to highlight, some of the differences between the results obtained through this work and the results obtained by Den Hartog and Ormondroyd [1]. A 0.01 rad amplitude base angular excitation was chosen as the system input.

To grid the $\{T_{f,\max}, \omega\}$ space for $I_d = 0.1\,\mathrm{kg\,m^2}$, the excitation frequencies ranged from 4.5 up to 4.99 in 0.01 rad/s increments. For this damper inertia, the primary system's resonant frequency will range from approximately 4.77 rad/s with $T_{f,\max} = \infty$, up to 5.0 rad/s with $T_{f,\max} = 0$. The damper friction was then chosen based on trial solutions and was selected to range from 0.22 to 0.4 N m, in 0.002 N m increments. The resulting steady-state displacements of the primary inertia in response to the base excitation are shown in Fig. 9 for points in the $\{T_{f,\max}, \omega\}$ space just described. In Fig. 9, the maximum responses at each friction level are connected and shown as the black curve through the peak frequency responses. Two white crosses are also shown in the figure and are used to indicate the locations of the maximum response location at the optimum friction level and the maximum response location at the friction level specified by Den Hartog and

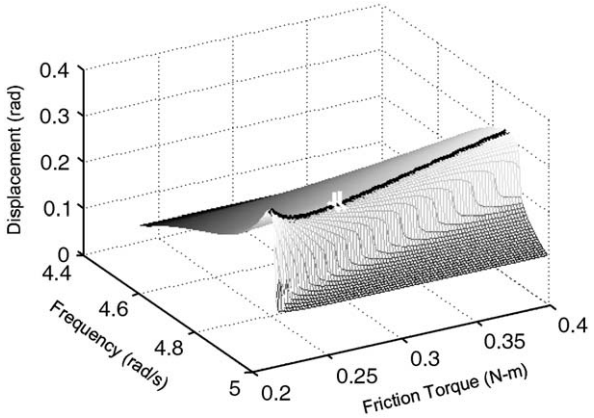

Fig. 9. Primary system steady-state angular displacement with 0.1 kg m^2 damper inertia.

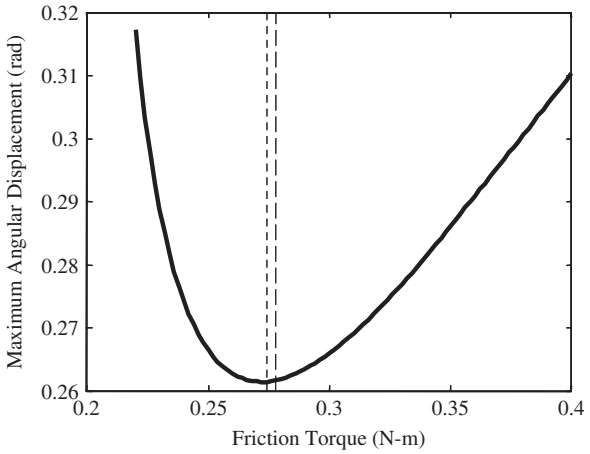

Fig. 10. Primary system maximum steady-state angular displacement as a function of damper friction with 0.1 kg m^2 damper inertia (– –, optimum friction; –·–, friction specified by Den Hartog and Ormondroyd [1]).

Ormondroyd [1]. The friction specified by Den Hartog and Ormondroyd is slightly higher than the actual optimum friction, although, as seen in Fig. 9, the two points (maximum response with optimal friction and maximum response with Den Hartog and Ormondroyd friction) are not very far apart, a reflection that, while not truly optimal, the friction specified by Den Hartog and Ormondroyd is quite close to the optimal value. This behavior is better seen in Fig. 10, where the locus of maximum responses at each friction level are shown plotted as a function of the friction torque. In this figure, the optimum friction is indicated by a dashed line, while the friction specified by Den Hartog and Ormondroyd is indicated by a dash–dotted line.

As noted previously, one assumption of Den Hartog and Ormondroyd was that the steady-state response of the primary system is nearly sinusoidal and will occur at the natural frequency of the primary system. This implicitly requires that the damper inertia be small relative to the inertia of the primary system. As such, with increasing mass ratios between the damper and primary system inertias, the assumption may not be as reasonable as for the case of a small mass ratio. To test this, the steady-state responses were determined for the cases of mass ratios of 0.2 and 0.5 (requiring damper inertias of 0.2 and 0.5 kg m^2, respectively). The steady-state responses as functions of frequency and damper friction are shown in Figs. 11 and 12 for mass ratios of 0.2 and 0.5, respectively. Due to the higher damper inertias, the excitation frequency range was extended down to 4.0 rad/s for these two tests. As in Fig. 9, the maximum responses at the optimum friction level and at the friction specified by Den Hartog and Ormondroyd are indicated by white crosses. In both cases, Den Hartog and Ormondroyd specify a higher friction level than is truly optimal. The corresponding plots of the primary

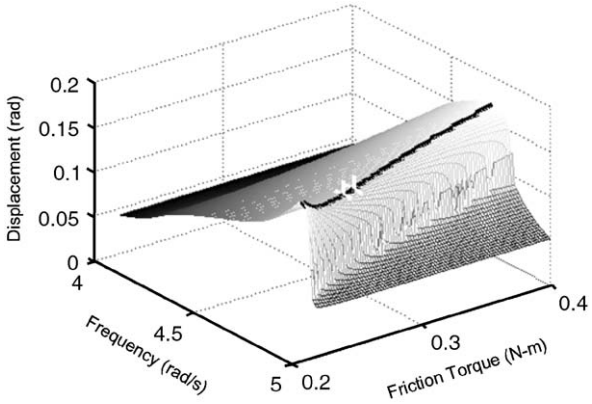

Fig. 11. Primary system steady-state angular displacement with 0.2 kg m^2 damper inertia.

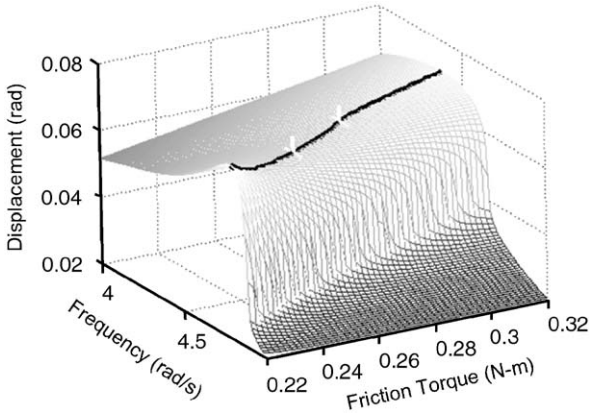

Fig. 12. Primary system steady-state angular displacement with 0.5 kg m^2 damper inertia.

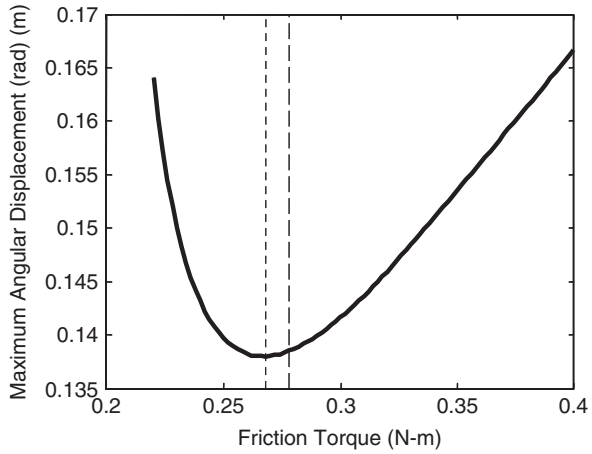

Fig. 13. Primary system maximum steady-state angular displacement as a function of damper friction with 0.2 kg m^2 damper inertia: – –, optimum friction; – · –, friction specified by Den Hartog and Ormondroyd [1].

system's maximum angular deflection at each friction level are shown in Figs. 13 and 14, with dashed and dash–dotted lines representing the optimum friction level and the friction specified by Den Hartog and Ormondroyd, respectively.

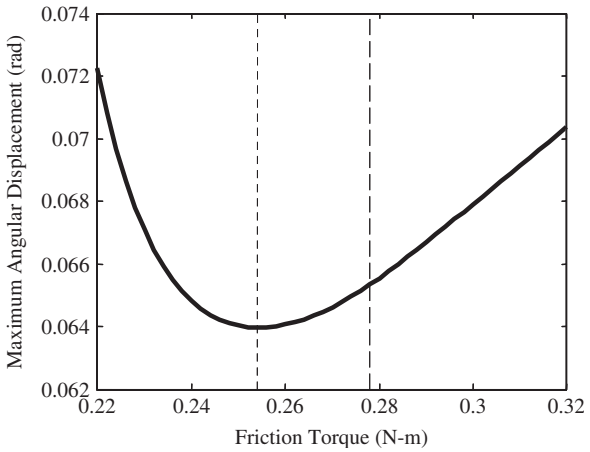

Fig. 14. Primary system maximum steady-state angular displacement as a function of damper friction with $0.5\,\mathrm{kg\,m^2}$ damper inertia: – –, optimum friction; – · –, friction specified by Den Hartog and Ormondroyd [1]).

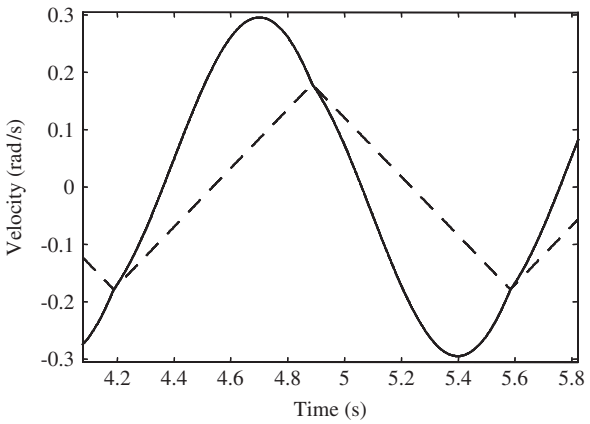

Fig. 15. Primary system and damper velocities during slip-only response with $0.5\,\mathrm{kg\,m^2}$ damper inertia and $T_{f,\max} = 0.256\,\mathrm{N\,m}$: —, primary system velocity; – –, damper velocity.

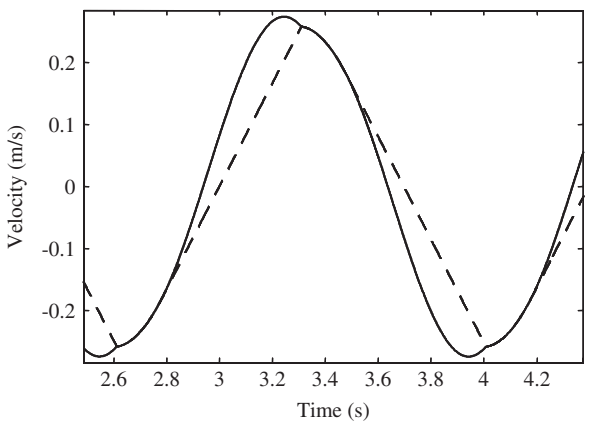

Fig. 16. Primary system and damper velocities during stick-slip response with $0.5\,\mathrm{kg\,m^2}$ damper inertia and $T_{f,\max} = 0.417\,\mathrm{N\,m}$: —, primary system velocity; – –, damper velocity.

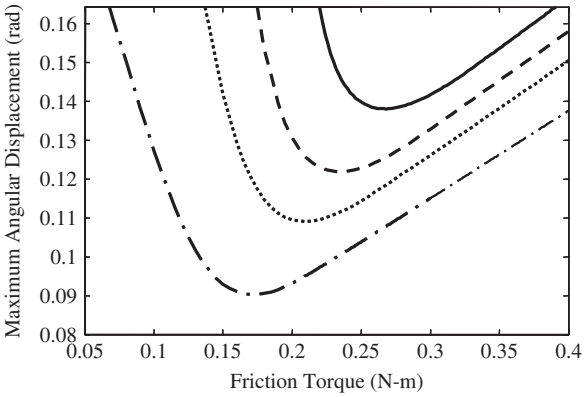

Fig. 17. Primary system maximum steady-state angular displacement as a function of damper friction with 0.2 kg m^2 damper: — undamped primary system, – –, 0.5% damping in primary system; …, 1% damping in primary system; –·–, 2% damping in primary system.

In examining the results shown in Figs. 13 and 14, it is apparent that as the mass ratio increases, the optimum friction becomes smaller than the value predicted by Den Hartog and Ormondroyd. In addition, the difference in performance achieved with the two different friction levels increases. As noted previously, one reason for this is that the steady-state solution is not truly sinusoidal, as assumed by Den Hartog and Ormondroyd. To examine this issue, the time domain responses of the primary system was determined for the case of the 0.5 kg m^2 implemented with two different friction levels; $T_{f,\max} = 0.256$ and 0417 N m. The steady-state velocities of the primary system and damper inertias are shown in Figs. 15 and 16 for these two friction levels, respectively. As seen in the figures, the 0.256 N m friction was sufficiently low to allow for a complete-slip response, while the 0.417 N m friction resulted in stick-slip behavior. In both figures, the steady-state velocity of the primary system is not a sinusoid. Rather, the steady-state response is, as expected, a series of repeating transient responses. This behavior is especially clear in the case of the stick-slip response shown in Fig. 16, although it can also be discerned in the slip-only response shown in Fig. 15.

Based on the steady-state responses shown in Figs. 15 and 16, the assumption of a sinusoidal response on the part of the primary system is not truly valid for the case of a damper with a finite inertia. A consequence of that result is that the friction specified by Ormondroyd and Den Hartog [1] is not truly optimal. However, the results also indicate that the performance does not vary significantly when a friction damper is designed with the truly optimal friction or with the friction specified by Den Hartog and Ormondroyd. For example, with a mass ratio of 0.2, the truly optimal friction and the friction specified by Den Hartog and Ormondroyd vary by less than 4% and result in performance variations on the order of 0.5%. It is important, however, that an exact analysis has been performed on the behavior of a vibrating system equipped with a friction damper for a number of reasons. First, the close agreement between the truly optimal friction and the friction specified by Den Hartog and Ormondroyd is a rigorous validation of the conclusions of these authors.

More importantly, however, the exact analysis permits the inclusion of viscous damping in the primary system. In the presence of viscous damping, the truly optimal friction can be quite different from the friction specified by Den Hartog and Ormondroyd. To demonstrate this, the optimum friction for a 0.1 kg m^2 damper applied to the primary system was determined. In this case, the primary system was as described above, but with the addition of viscous damping. The optimum damper friction was determined for the cases of the primary system with 0.5%, 1%, and 2% damping ratios. The maximum response of the primary system as a function of damper friction is shown in Fig. 17 for these different damping ratios, along with the maximum response for the case of an undamped primary system (similar to Fig. 10). As seen in Fig. 17, inclusion of damping in the primary system dramatically changes the response of the system. The optimal friction levels are now significantly smaller than the values predicted by Den Hartog and Ormondroyd and substantial performance improvements should be realized by implementing the true optimum friction in the place of the earlier predicted value.

In light of the potential improvements that are predicted by this new analysis, future work will focus on experimental verification of the results. To this end, the implementation of friction dampers on primary

systems with finite equivalent viscous damping is currently under way. The analysis presented in this paper has thus formed a foundation for future work in this area and will hopefully lead to more flexible implementation of friction dampers to vibrating systems in the future.

5. Conclusions

A new approach to the analysis of friction dampers has been presented in this work. The exact form of the steady-state solution for a friction damper implemented on a primary system was developed and numerical solutions to the resulting sets of nonlinear equations were obtained for different friction levels. The results were used to determine the optimum friction level in a friction damper applied to a specific primary system. When compared to classical results presented by earlier authors, the new approach provides a more optimal solution, although the corresponding performance improvements are not significant in most cases. The new approach is an improvement over past works in this area, however, in that viscous damping in the primary system may be accommodated. When viscous damping is included in the primary system, substantially different results are obtained with the new analysis approach. These results show the potential for the new analysis approach to serve as a guide in designing more optimal friction dampers.

References

[1] J.P. Den Hartog, J. Ormondroyd, Torsional vibration dampers, *Transactions of the American Society of Mechanical Engineers, Applied Mechanics Division* APM52-13 (1929) 133–152.
[2] S. Ye, K.A. Williams, Semi-active control of torsional vibrations using an MR fluid brake, *Proceedings of SPIE* 5390 (2004) 135–146.
[3] S. Ye, K.A. Williams, MR fluid brake for control of torsional vibration, SAE Paper 2005-01-1503, *SAE 2005 World Congress and Exhibition: Experiments in Automotive Engineering*, April 12, 2005.
[4] W. Ker Wilson, third ed. (three volumes), *Practical Solution of Torsional Vibration Problems*, Wiley, New York, 1956.
[5] W.A. Tuplin, *Torsional Vibration: Elementary Theory and Design Calculations*, Wiley, New York, 1956.
[6] E.J. Nestorides, *A Handbook on Torsional Vibration*, Cambridge University Press, New York, 1958.
[7] M.R. Jolly, J.W. Bender, J.D. Carlson, Properties and applications of commercial magneto-rheological fluids, *Journal of Intelligent Material Systems and Structures* 10 (1) (2000) 5–13.
[8] D. Carlson, D.M. Catanzarite, K.A. St. Clair, Commercial magneto-rheological fluid devices, *International Journal of Modern Physics B* 10 (23-24) (1996) 2857–2863.
[9] A.V. Srinivasan, D.M. McFarland, *Smart Structures:, Analysis and Design*, Cambridge University Press, New York, 2001.